Micron 135 (2020) 102874

Contents lists available at ScienceDirect

Micron

journal homepage: www.elsevier.com/locate/micron

Evaluating fidelity of CT based 3D models for Zebrafish conductive hearing system

Jordi Marcé-Nogué[a,b], Juan Liu[a,*]

[a] Department of Pathology and Anatomical Sciences, Jacobs School of Medicine and Biomedical Sciences, University at Buffalo, State University of New York, NY, USA
[b] Institut Català de Paleontologia Miquel Crusafont, Universitat Autònoma de Barcelona, Cerdanyola del Vallès, Barcelona, Spain

ARTICLE INFO

Keywords:
Zebrafish
Weberian apparatus
CT imaging
Finite element analysis

ABSTRACT

The zebrafish Weberian apparatus is an emerging model for human conductive hearing system. Their Weberian apparatus comprises minute bones and ligamentary links, and conducts sound pressure transmission from the gas bladder to inner ear through four pairs of Weberian ossicles along the vertebral column. We herein present a methodological study using MicroCT to image the Weberian apparatus for biomechanical and morphological analysis. The aim of this work is to evaluate computational models generated from multiple MicroCT scans with different parameters, to identify the most feasible scan combination for practical (minimized scan time) yet accurate (relative to highest resolution) biomechanical simulations. We segmented and created 3D models from CT scan image stacks at 4.64 μm, 5.05 μm, 9.30 μm and 13.08 μm voxel resolutions, respectively. Then, we used geometric morphometrics analysis to quantify inter-model shape differences, as well as a series of finite element modal and harmonic analyses to simulate auditory signal vibrations. Relative to the highest resolution and most accurate model, the Model 9.30 is closest in overall geometry and biomechanical behavior of all lower resolution models. The differences in resolution and quality of the CT substantially affect the segmentation and reconstruction process of the three-dimensional model of the ossicles, and the subsequent analyses. We conclude that scan voxel resolution is a key factor influencing outcomes of biomechanical simulations of delicate and minute structures, especially when studying the harmonic response of minute ossicles connected by ligaments using finite element modeling. Furthermore, contrast variations in CT images as determined by x-ray power and scan speed, also affect fidelity in 3D models and simulation outcomes.

1. Introduction

Zebrafish (*Danio rerio*) is a versatile model organism in biomedical and organismal biology research. Studies using osteological elements of zebrafish with the aid of various imaging tools have seen a dramatic increase in recent years, towards improved understanding of the normal function and pathological consequences in diverse areas such as musculoskeletal systems (Fleming et al., 2005; Harris et al., 2014; Weigele and Franz-Odendaal, 2016), developmental characteristics (Bird and Mabee, 2003; Cubbage and Mabee, 1996; Siomava et al., 2018), vertebrate evolution (Hernandez et al., 2007), hormone disorders (Brown, 1997; Keer et al., 2019), environmental toxicity (Baker et al., 2013), and others. Whereas zebrafish has been widely used as model organisms in investigations of the genetic basis and sensorineural aspects of hearing (Blanco-Sánchez et al., 2017; Nicolson, 2017; Whitfield, 2002), computational modeling of bony structures in its conductive auditory system is an emerging and promising direction in hearing research.

The Weberian apparatus in zebrafish conducts sound pressure transmission from gas bladder to inner ear through Weberian ossicles, and is analogous to the human middle ear, which conducts sound vibration and transmit sound pressure from the temporal membrane to the inner ear through three middle ear ossicles (Evans, 1925; Weber, 1820). Previous research using behavioral features and evoked potential audiograms have shown that fishes with Weberian apparatus (otophysians) have increased hearing range compared to those without (Ladich and Fay, 2013; Ladich and Wysocki, 2003; Lechner and Ladich, 2008; Popper, 1972). Developmental biology evidence of zebrafish hearing suggests that the Weberian ossicles gradually increase the range of frequencies available to the inner ear during zebrafish growth, just as middle ear development increases frequency range in mammal ontogeny (Higgs et al., 2003). Furthermore, Weberian ossicles conduct sound pressure from gas filled bladder to the fluid filled sinus impar of

* Corresponding author at: Department of Pathology and Anatomical Sciences, Jacobs School of Medicine and Biomedical Sciences, University at Buffalo, State University of New York, NY, USA.
E-mail address: liujuan@berkeley.edu (J. Liu).

https://doi.org/10.1016/j.micron.2020.102874
Received 16 December 2019; Received in revised form 4 April 2020; Accepted 5 April 2020
Available online 22 April 2020

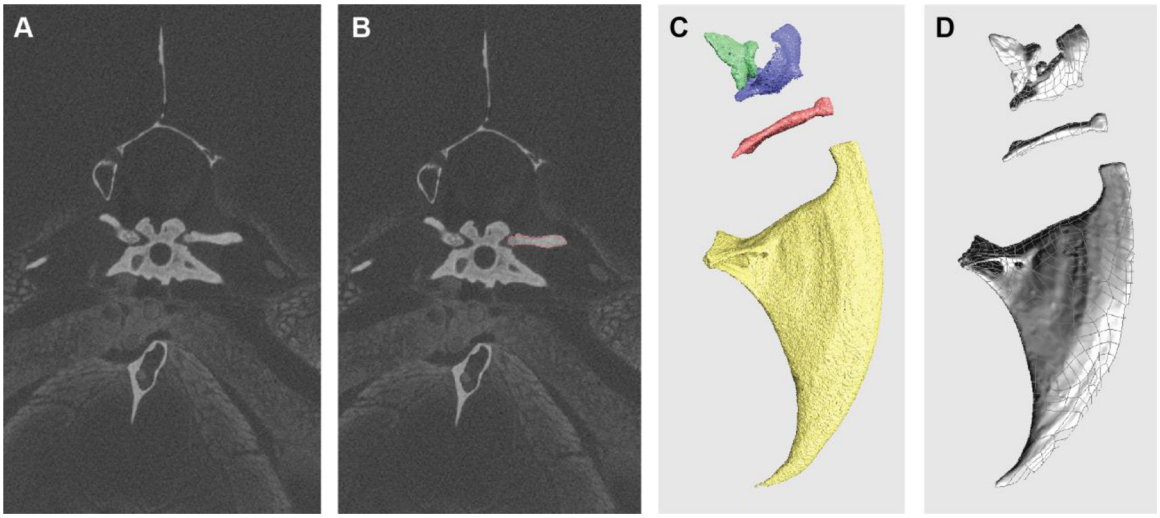

Fig. 1. A) reconstructed image slice (cross-sectional view) of zebrafish from MicroCT scan; B) Contour detected (in red) intercalarium bone using Amira build-in algorithm; C) STL model obtained after the segmentation; D) CAD file after smoothing and repairing the STL model.

the inner ear (Popper and Fay, 2011; Retzius, 1881). This particular conduction pathway is functionally analogous to the air-bone-fluid conduction system of the middle ear ossicles of human. Therefore, the Weberian ossicles chain in zebrafish is an ideal structural system for modeling auditory sound conduction in humans.

Weberian ossicles are developmentally derived from elements of the first four vertebrae in zebrafish. These minute bones form an ossicles chain along with associated ligaments. The paired ossicle chains are located bilaterally to the vertebral column. From anterior to posterior, the ossicles are claustrum, scaphium, intercalarium, and tripus (Fig. 1). The tripus is connected to the anterior portion of the gas bladder via ligaments, while the scaphium and claustrum are coupled to the inner ear fluid space (the atrium of the sinus impar). The Weberian ossicles mechanically couple vibrations of the gas bladder induced by sound to the inner ear fluid, allowing sound to be transduced into electrical signals by the sensory cells of the inner ear.

Morphological characteristics of Weberian ossicles have been studied from the perspectives of skeletogenesis (Fisher and Mabee, 2004), development (Bird and Mabee, 2003), ontogeny (Grande and Young, 2004), growth (Bird and Hernandez, 2009), and response to hormone levels (Keer et al., 2019). Two previous biomechanical studies on the Weberian apparatus also elucidated functional morphological traits of Weberian ossicles (Alexander, 1962; Finneran and Hastings, 2000). Microscopic dissection, clearing and staining methods, histological slice, and two-dimensional (2D) radiograph were extensively used in previous research to investigate and capture the morphology of Weberian ossicles. These classical yet prevalent methods are essential and accurate to examine and image morphology of Weberian ossicles. However, in order to quantify the shape and build three-dimensional (3D) models to understand the mechanism of this sound conductive system, we aim to leverage an imaging modality allowing for the characterization of ossicles and related structures in calibrated 3D, natural shape, orientation, and spatial intra-relationships and inter-relationships with surrounding structures (ligament, gas bladder, and fluid sac).

Techniques including magnetic resonance imaging (MRI) and computed tomography (CT) allow the non-invasive 3D visualization of external and internal structures at different resolutions from cells, to organ system, and whole organism levels (Cheng et al., 2011; Walter et al., 2010). CT scans uses x-ray technology with a small dose of ionizing radiation whereas MRI uses radio waves and powerful magnets to produce images. In general, CT scans are more powerful for obtaining high-contrast images of bony structures, whereas MRI capture better images on soft tissues, joints, tendons and ligaments. However, the Weberian apparatus consist of minute bony structures (ossicles) and non-mineralized tissues (ligament). Fortunately, limits CT scanning for non-mineralized tissue is compensated with histological staining prior to scan (Babaei et al., 2016; Metscher, 2009), which make CT more appropriate to our imaging needs. Moreover, with dramatic technological advances in the past decade, lab-based or commercial MicroCT (versus Synchrotron radiation CT, SrCT) is now efficient, cost-effective, and high accurate in generating calibrated 3D image data, and should potentially meet our imaging requirements.

Previous studies utilizing CT imaging techniques on zebrafish include SrCT analysis to model biomineralization in teeth and skeleton (Neues et al., 2006), contrast-enhanced MicroCT for monitoring the regeneration of cardiac tissue, MicroCT-based methods for phenotyping (Hur et al., 2017), and SrCT scan at sub-micro resolution and 3D whole organism image for histotomography (Ding et al., 2019). Here we present a study using MicroCT to image the Weberian apparatus for biomechanical analysis. The aims of this project are two-fold: 1) evaluate models generated from multiple MicroCT scans with different parameters to find the most feasible scan combination for practical yet accurate images for biomechanical simulations; 2) hypothesize practical scan parameter combinations for similar-sized structures in zebrafish, or the same structure in other small animal models.

2. CT scan to 3D model workflow

Functional morphology studies use reverse engineering concepts to understand biological structures and explore the relationships of function and form. Whereas forms can be quantified by computational morphological analytical methods such as geometric morphometrics (GMM) (Polly et al., 2016), functions are evaluated by biomechanical modelling techniques, for instance finite element analysis (FEA) (Rayfield, 2007), computational fluid dynamics (CFD) (Rahman, 2017) and multi-body dynamic analysis (Curtis, 2011). All of these methodologies require sufficiently accurate and complete morphological and anatomical data. Image stacks generated from X-ray based CT scan of biological structures are ideal to visualize, and then segmented into 3D models. Although there are a number of workflows and software available to utilize CT data for different purposes (Sutton et al., 2016), the general steps of converting CT images into 3D models follow the workflow as below.

2.1. Image segmentation

Image segmentation is used to locate region of interest (ROI) and

build 3D digital models, after CT image stack are reconstructed from the raw projection data generated by specimen scanning. Image segmentation is a technique in digital image processing and analysis to partition an image into multiple parts or regions to identify regions of interest (ROI). Image segmentation could involve separating foreground from background, or clustering regions of pixels based on similarities in grayscale or shape. There are two types of segmentation: manual and algorithm-based automatic segmentations. Different algorithms and techniques for image segmentation have been developed using domain-specific knowledge to effectively segment ROI. These applications include medical imaging, automated driving, video surveillance, and machine vision. However, segmentations of biological data for high fidelity models usually require additional manual adjustment because of structural complexity. In our current project, we used a built-in segmentation algorithm in the software Amira 6.0 to analyzes each image based on grayscale thresholding (Fig. 1a), then went through each image slice to ensure the ROI was accurately segmented (Fig. 1b). ROI from every slice are subsequently combined into 3D geometry and saved as stereolithography (STL) file, which is a raw 3D geometry composed of a mesh of triangles with coordinates for nodes and vertices (Fig. 1c). There are a number of self-developed, open source (e.g., 3D Slicer), and commercial software (e.g., Mimics, Avizio, Dragonfly etc.) available for CT image segmentation.

2.2. Geometry refinement

There are often defects in the geometry of STL file, which are usually caused by the orientation of the scanning and the precision of the scanner. For refinement, smoothing and element reduction procedure is usually performed. As it is observed in Fig. 1d, the segmented geometry has non-biological irregularities on the surface. That geometry was cleaned and smoothed at very low level to fulfill requirements of quality and consistency, without modifying its original morphology. The “quality” here refers to shapes of the triangular elements in the STL mesh that is measured by skewness or aspect ratio (Weatherill et al., 1998), whereas the “consistency” is to avoid possible topological errors with smooth operations.

2.3. STL versus CAD models

Most of biomechanical and morphological analysis can be performed with STL files. STL file, displayed as a mesh of triangles, describes the surface geometry of a three-dimensional object without color, texture or other model attributes. Models built in STL format are usually relatively smooth. STL formats are an excellent file option for 3D anatomical visualization and morphological analysis using morphometrics, because STL models can provide sufficient fidelity for shape analyses (Engelkes et al., 2019; Marcy et al., 2018).

However, for biomechanical analyses such as FEA and CFD, some researchers generate a CAD (Computer-Aided Design) solid model from the STL mesh (Barbero and Ureta, 2011). A CAD model is a vector-graphic standard for three-dimensional design used in mechanical design and engineering, unlike STL format file which involves triangulation of the geometry. CAD models can avoid possible mathematical errors caused by presence of non-biological angles in the geometry. CAD models (file type IGS or STP) have the boundary formed by curved surfaces using interpolation methods. CAD files also contain data for Non-uniform rational basis spline curves (NURBS) and surfaces (Piegl and Tiller, 1997). These are mathematical representations of the curves or surfaces which are smoother and maybe more accurate than that of STL file which depends on the number of triangles or cloud points. Therefore, we prefer CAD files for the biomechanical simulations in this study.

2.4. Model Accessibility

As a common good practice in scientific research to advance knowledge based on open flow of information, access to image stack from X-ray based CT scan as well as 3D models should be facilitated. Data underlying a published study should deposited in a suitable repository, and many researchers are already doing so. Although there is currently no agreement on how much and what type of data should be made available for studies using digital morphology, Davies et al. (2017) propose a set of recommendations for minimum standards and best practice for three-dimensional digital data publication. These recommendations include the availability of all the data upon publication in accessible standard formats and with a standard copyright license. This license should cover terms to specify ethical use and degree of commercial activities or modification allowed based on the shared data. The goal should be to allow research replication while crediting the source properly.

3. Material and Methods

3.1. Materials

A fixed and 70% ethanol preserved wild adult zebrafish, *Danio rerio*, KU 22656, was loaned from Division of Ichthyology, Biodiversity Institute, University of Kansas (KU). It was stained in 0.3% phosphotungstic acid in 70% ethanol prior to CT scan following the procedure described by Metscher (2009). Euthanization, dissection and observation of laboratory fishes in this study proceeded under protocol PTH04058N, reviewed and approved by the Institutional Animal Care and Use Committee, University at Buffalo.

3.2. CT scanning

A single specimen of an adult zebrafish (*Danio rerio)* was scanned using four different parameters and using two different MicroCT scanners (Table 1) in the Institute of Biotechnology, Cornell University (Ithaca, NY, USA).

The Xradia Zeiss VersaXRM-520 CT scanner uses proprietary interchangeable focusing optics that allows users to locate and scan small sub-regions within a specimen as large as 30 cm in height and 30 cm in diameter. This is followed by seamless digital stitching of multiple scanned sub-regions. On the other hand, Bruker Skyscan 1276 scanner is more cost-effective and time-efficient, using lower radiation doses and producing lower resolution scans.

The original measured length of the Weberian apparatus of the specimen is 2.59 mm (Fig. 2D). For further comparison, we compute a factor called “resolution factor” (length of Weberian ossicles chain/ Voxel size), which describes the number of slices needed to cover the

Table 1
Parameters of the four different scans regarding voxel size, power, speed of scan, and computed Resolution Factor.

MODEL	VOXEL SIZE [μm]	CT	radiation energy	Scan speed	Resolution Factor
Model 4.64	4.64	Xradia Zeiss VersaXRM-520	100kV, 9 W	1601 images/4S/exposure	558.2
Model 5.05	5.05	Bruker Skyscan 1276	55kV, 200 micro amps	900 images/675 ms/exposure	512.9
Model 9.30	9.30	Xradia Zeiss VersaXRM-520	100kV, 9 W	1601 images/4S/exposure	278.5
Model 13.08	13.08	Xradia Zeiss VersaXRM-520	100kV, 9 W	1601 images/4S/exposure	198.0

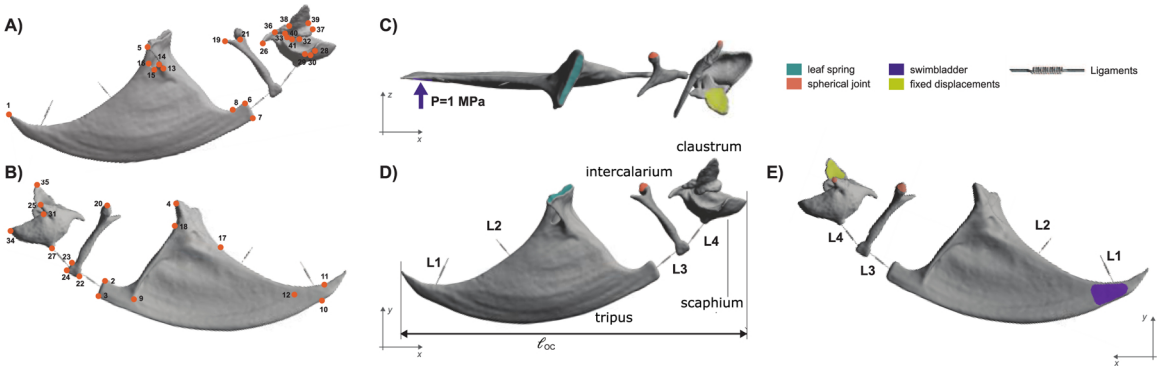

Fig. 2. Geometry and model boundary condition of Weberian apparatus. A) Lateral view and B) Medial view with the 41 landmarks used in the geometric morphometrics analysis. C) Dorsal view, D) Lateral view and E) Medial view with the loading area, fixed conditions areas, and spring-based ligaments of the FEA model. Orange dots labeled with numbers 1- 41, landmark 1 through 41; L1 through L4, Ligament 1 through 4; Loc, length of Weberian ossicles chain.

body of the Weberian apparatus (Table 1). This is a comparable index applicable in evaluating scans of other structures and differently sized fishes.

3.3. Segmentation and reconstruction

CT images were imported to the software Amira 6.0 (Thermo Scientific, Houston, TX, USA) to perform a region of interest (ROI) segmentation. The scan was segmented using threshold selection and manual adjustment. To eliminate the variability of different users, segmentations for all models were performed by the first author who has decades of experience in segmenting biological structures from CT images. 3D surface model was built from segmentations for the four ossicles of the Weberian apparatus: claustrum, scaphium, intercalarium and tripus respectively.

Irregularities in the surface resulting from segmentation to model conversion were repaired using refinement and smoothing tools of Geomagic Wrap (3D Systems, v. 12, Rock Hill, SC, USA). All models were oriented using the best-fit alignment tool (with default settings) within Geomagic Wrap to ensure that the four models are equally aligned. Models then were converted to a CAD files for further analysis (Marcé-Nogué et al., 2011).

3.4. Geometric Morphometrics analysis

We collected 41 landmarks in cartesian coordinates on the surface of the Weberian apparatus of the 4 different models. These coordinates were analyzed using the 'geomorph' R package (Adams and Otárola-Castillo, 2013) and are available in the document S1 of the Supplementary information. A Procrustes superimposition was performed to remove the differences due to scale, translation, and rotation, leaving only variables directly related to shape. Next, these shape variables were visualized for morphological differences among models using principal component analysis (PCA).

3.5. Finite Element Analysis (FEA)

FEA (specifically, modal and harmonic response analyses) were performed to study the biomechanical performance of the ossicles of the Weberian apparatus using the finite element package ANSYS 17.1 (Ansys, Canonsburg, USA) and a Dell Precision Workstation 7820 with 64 GB RAM, and 16 cores Intel(R) Xeon(R) Silver 4110 processor. Modal and harmonic response analyses were performed in all four models respectively (Table 1) to evaluate the influence of the image quality/resolution towards FEA outputs. The 3D geometry models were solid meshed using the ANSYS mesh module with an adaptive mesh of tetrahedral elements (Marcé-Nogué et al., 2015). The mesh of the model consists of approximately 300,000 elements that will be used in FEA. Note that the FEA mesh is different from that of a STL mesh because the FEA mesh covers the inner thickness of the model in addition to representing the surfaces.

Material properties defined in these analyses were adopted from previous FEA publications: Young modulus 16 GPa (Soons et al., 2010); coefficient of Poisson 0.3 (Areias et al., 2016; De Greef et al., 2017; Funnell et al., 1992); density of the bone 2100 g/cm3 (De Greef et al., 2014; Alexander, 1959). Boundary conditions were defined in the model to constrain the movements that the ossicles of the Weberian apparatus experience during simulated function (Fig. 2). Four ligaments were included in the model (Alexander, 1962) with rigidity of the ligament set at 1.5 N/mm (De Greef et al., 2017, 2014). Furthermore, the direct contact of the ossicles with the vertebra has been defined using three different types of connection: spherical joints, leaf spring, and a total fixation. Moreover, the cushioning capsule of Weberian ossicles is defined as Rayleigh damping $\beta = 0.0001$ s and $\alpha = 0$ Hz (Areias et al., 2016; Caminos et al., 2018; De Greef et al., 2014; Volandri et al., 2011), and elastic stiffness $K_{cush} = 0.0025$ N/mm^3 (Marcé-Nogué and Liu, *in prep*). Lastly, a force of 0.001 N was applied to obtain the nominal unitary harmonic response in the tip of the tripus where the gas bladder contacts the ossicle. A sweeping analysis of frequency values was conducted between 10 Hz and 10000 Hz. We sampled the amplitude of the displacement and the velocity and its phase from 200 points regularly distributed throughout the different ossicles.

4. Results

4.1. Qualitative comparison of segmented 3D models

The 3D geometry models obtained after the segmentation, and the CAD files after the conversion process, are shown in Fig. 3A, 3B, 3C and 3D. Generally speaking, the larger the structure, the less the difference between models. Model 4.64 shows a complete Weberian apparatus with all the ossicles details, whereas the other three models show more or less incompleteness in the claustrum and the foramen at the superior process of the tripus. On the other hand, the overall shape of the tripus exhibits no visual differences across models.

4.2. Quantitative comparison of the models using geometric morphometrics

In quantitative comparison, there are slight differences between the models in the volume and surface area of each ossicle (Table 2). There is a general trend towards smaller values in models built from higher resolution data. The most apparent differences can be found in the scaphium; regions of the scaphium are incomplete in Models 5.05 and 13.08.

The Model 4.64 is the most accurate model (supported by observation from dissection and the visualization of CT images), so that

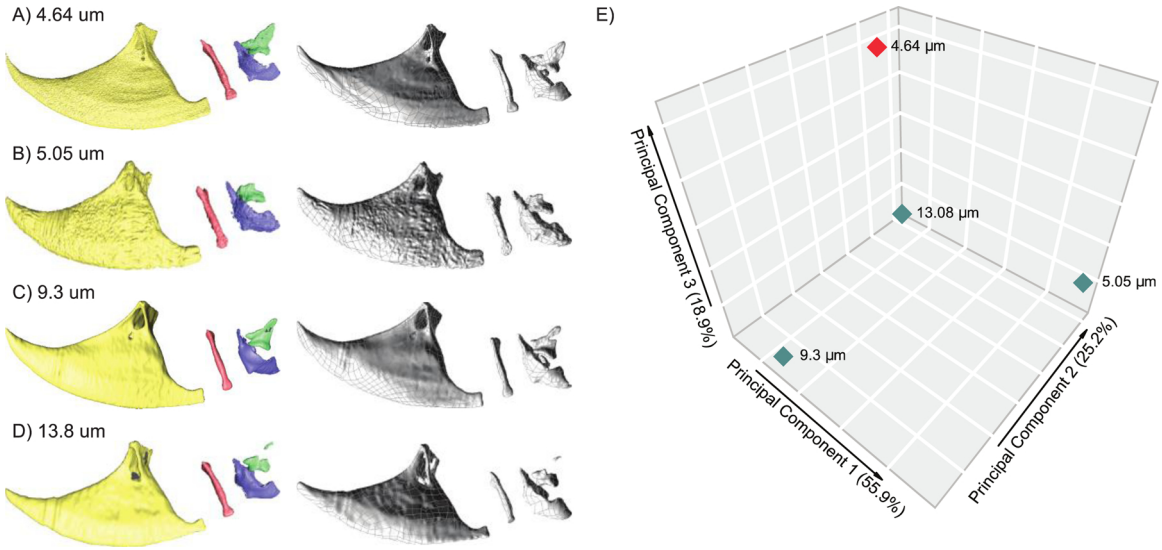

Fig. 3. Geometry obtained after segmentation in .stl format (left) and CAD format (right) for A) Model 4.64 B) Model 5.05 C) Model 9.30 and D) Model 13.8; E) Morphospace of the first three morphometric PCs occupied by the four models.

Table 2
Differences in the computed volume (mm3) and area (mm3) of the Weberian ossicles for the four different models

	Tripus	Intercalarium	Scaphium	Claustrum
VOLUME [mm3]				
Model 4.64	0.047629	0.03271	0.09803	0.01949
Model 5.05	0.066382	0.03439	0.01324	0.01912
Model 9.30	0.047104	0.02819	0.09725	0.01886
Model 13.08	0.044479	0.02601	0.01025	0.01415
SURFACE [mm2]				
Model 4.64	2.1791	0.20011	0.51465	0.15424
Model 5.05	2.1185	0.20534	0.50924	0.10057
Model 9.30	1.9906	0.18131	0.49825	0.12438
Model 13.08	1.9152	0.15776	0.44941	0.08216

this model is served as a reference point for comparison with the remaining models. PCA of the morphometric data resulted in three PCs that summarize 100% of the variance (Fig. 3E). The Procrustes distance to the reference model is 0.084 for the Model 5.05, 0.062 for the Model 9.30, and 0.061 for the Model 13.08. This result suggests that in spite of relatively high-resolution factor, the Model 5.05 is the least accurate for replicating the highest resolution model.

With the loadings of each landmark (components x, y, and z separately), we calculate the contribution of each landmark vectorially summing the x, y, and z loadings. Then, we sum the total contribution of each landmark vectorially summing the contribution in PC1, PC2 and PC3 to obtain the most influential landmarks in the shape differences. The landmarks that vary the most among the four models are the landmark 23, 8, 33, 40, 22 and 24, which help pinpoint the principal morphological differences between models built from scans of different resolutions. These landmarks are mostly located in the tip of the intercalarium where the ligaments are attached and in the contact areas between the scaphium and the claustrum. Given the variations at such important loci, the fidelity of the models may affect the subsequent biomechanical analysis.

4.3. Biomechanical comparisons using FEA

Given the modal analysis is mathematically mandatory before the harmonic analysis, it was performed first. Table 3 reports the first six modes of vibration for each model obtained in the modal analysis. There are only minor differences in the first two modes among all the models, but substantial differences between models in Mode 3, 4, 5, and 6.

Table 3
Frequencies of the first six modes of vibration obtained for each model

MODEL	MODE 1 [Hz]	MODE 2 [Hz]	MODE 3 [Hz]	MODE 4 [Hz]	MODE 5 [Hz]	MODE 6 [Hz]
Model 4.64	866	1009	1270	21796	33084	37558
Model 5.05	874	1040	2213	19698	44134	68841
Model 9.30	796	1057	1214	17228	28361	37966
Model 13.08	823	1036	1142	17956	36968	40548

Harmonic analysis results characterize the response of the Weberian ossicles to the sound pressure exerted by the gas bladder (Fig. 4). Results for tripus, intercalarium and scaphium were recorded in the simulations. Claustrum is not included in the analysis because no independent response is expected, as claustrum is described as being fused to the first vertebra to support the wall of the sinus impar atrium, and thus immobile in zebrafish (Bang et al., 2001).

A resonance peak at around 900 Hz is present in all models. The differences among the amplitude of the intercalarium and the scaphium are more apparent than that among tripus. The amplitude of the vibration of the scaphium in Model 5.05 is unexpectedly and abnormally low, compared to that of other models. Both Model 9.30 and 13.08 generate tripus resonance and peak amplitude frequencies close to that of the Model 4.64. In contrast, intercalarium and scaphium values for the same models diverge from each other. The tripus vibrations are nearly in phase in all of the models (Fig. 4). Intercalarium vibrations of Model 13.08 are out of phase, whereas scaphium vibrations of Model 5.05 are out of phase comparing to the rest. Using the highest fidelity Model 4.64 as a reference, ossicles of Model 9.30 are all relatively in phase except moderate shift in intercalarium values at high frequencies. The overall behavior of Model 9.30 in both modal analysis (Table 3) and harmonic analysis (Table 4, Fig. 4) is closest to Model 4.64 out of the three remaining models.

5. Discussion

Morphological and biomechanical differences are evident from comparative analyses of four zebrafish Weberian apparatus models with varying scanning resolutions. The first important difference between models are the completeness of the Weberian ossicle models derived

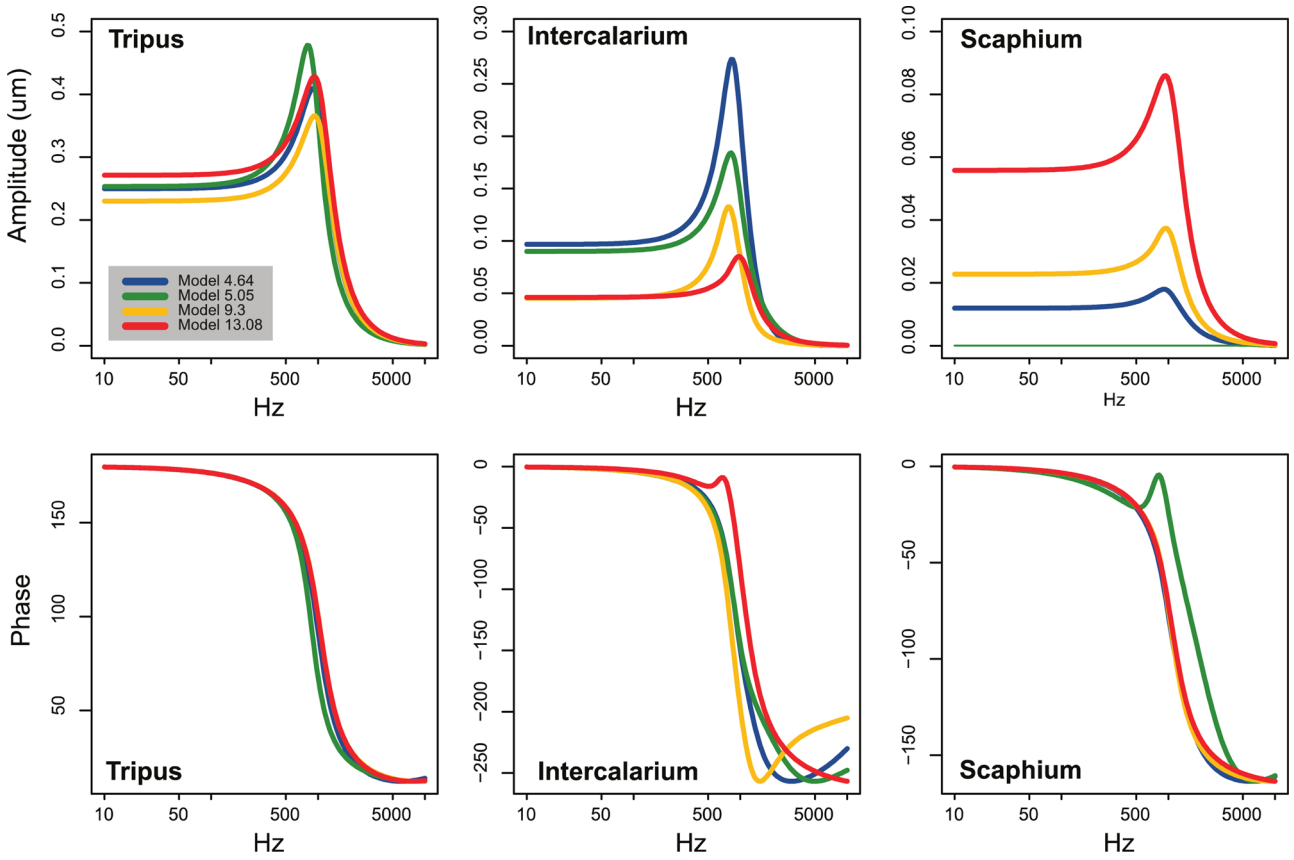

Fig. 4. Harmonic response between 10 and 10000 Hz in the tripus, intercalarium and the scaphium under the application of a 1 Pa pressure in the contact area of the gasbladder with the tripus. X axis is responding frequency displayed in logarithmic scale, Y axis is amplitute and vibration phase of three ossicles respectively. Note the scaphium of Model 5.05 does not resonant (upper right figure), which explained the unexpected low value in Table 4. Also note, intercarlarium of Model 13.08 and scaphium of Model 5.05 are out of phase (lower middle and right).

from segmentation. Model 4.64 shows the most complete Weberian ossicles chain, whereas the other three models exhibit incomplete portions on the claustrum and the scaphium. These differences are potentially responsible for differences in FEA outputs in terms of boundary condition variability. For example, the missing area on the dorsal surface of the claustrum, where movement constraint was applied, could result in different displacement patterns compared to constraints placed on a model with complete morphology. Also, missing part of the scaphium, where a joint is supposed to be located, could have resulted in varying model behavior because of different joint angles created in models with incomplete morphology. These important differences may explain the low fidelity of Model 5.05 outputs in both GMM analysis and harmonic response.

Quantitative geometric comparisons reveal anatomically and functionally important differences in the models built from varying scan resolutions. Apparent differences were detected at the landmarks 22, 23 and 24 from GMM analysis. These landmarks are located in the areas where the ligaments 3 and 4 are connected to the intercalarium. These variations are in an important location, where the vibration of the tripus is transmitted via the ligaments to the intercalarium and to the scaphium. It can be an important factor which may contribute to differences in the simulated harmonic responses of the intercalarium (Fig. 4).

Biomechanical simulation outputs also differ among models and among bony elements of the hearing system. The harmonic response in the tripus is the least affected from the effect of scan resolution, likely because tripus is the biggest ossicle and least affected in geometry. Therefore, comparisons of biomechanical performance in tripus alone, without considering the transmission of the vibration to the other ossicles, appear to be immune to the effects of CT scan resolution.

The quality of the CT-scans for morphological models has been discussed in previous studies, and the conclusion was that low-resolution scans can provide a sufficiently accurate geometry for 3D shape analyses (Marcy et al., 2018). Also, models built from more time-efficient, lower-resolution scans may provide valid results in a comparative context when perform static FEA (McCurry et al., 2015). This could be true for analysis on larger structures such as jaw bones (comparing to the minute ossicles). However, our results show that the dynamic

Table 4
Frequency of resonance and peak amplitude of the harmonic response in each model.

	Tripus		Intercalarium		Scaphium	
MODEL	**Frequency [Hz]**	**Amplitude [μm]**	**Frequency [Hz]**	**Amplitude [μm]**	**Frequency [Hz]**	**Amplitude [μm]**
Model 4.64	912	0.4089	821	0.2732	912	0.0180
Model 5.05	793	0.4778	821	0.1840	1084	0.0001*
Model 9.30	944	0.3657	766	0.1325	944	0.0374
Model 13.08	912	0.4281	977	0.0851*	944	0.0860

* indicate unexpected low or high value comparing to Model 4.64.

analysis (modal analysis and harmonic analysis) of FEA require high CT scan resolutions for more resolved models. The morphological fidelity of a model generated from CT images is affected by two main factors. One is the quality of segmentation, which require anatomical expertise on the structure that being segmented. The other factor is the resolution and quality of CT scan. In this project, the quality of segmentation is controlled by segmenting the structure by the same person, using the same software, computer, protocol, and criteria. The differences observed in the morphological and biomechanical analyses largely resulted from the resolution of CT scans and contrast of CT images.

To conclude, 3D models of zebrafish conductive hearing system are segmented from CT scans at four voxel resolutions (4.64 μm, 5.05 μm, 9.30 μm and 13.08 μm voxel resolutions). Overall, CT scans with contrast at high voxel resolution (below 20 μm) is very promising for 3D visualization and biomechanical simulations of delicate and minute structures like Weberian ossicles and associated structures. Whereas the highest-resolution model (Model 4.64) is most accurate in reproducing complete morphology according to qualitative observations, the Model 9.30 is closest to Model 4.64 based on geometric morphometric comparison and harmonic responses. Model 5.05, despite very fine voxel resolution, is least accurate in geometry which leads to low fidelity of output of harmonic responses. We believe the low fidelity of Model 5.05 is related to time-efficient and lower-dose radiation scan (Table 1). The resolution factor of the model with acceptable fidelity (Model 9.30) is around 300 (about 300 slices capturing the Weberian ossicle chain along the long axis; Table 1). Similar resolution considerations are recommended for future image-based analyses of Weberian apparatus, as well as similarly sized organ or structure systems in zebrafish.

CRediT authorship contribution statement

Jordi Marcé-Nogué: performed analyses and wrote manuscript.**Juan Liu:** captured the idea collected data performed analyses and wrote manuscript.

6. Declaration of interests

The authors declare that they have no known competing financial interests or personal relationships that could have appeared to influence the work reported in this paper.

Acknowledgments

The authors thank Andy Bentley, Leo Smith, and Gloria Arratia (University of Kansa) for specimen loan; Jack Tseng for stylistic improvement; Teresa Porri (University of Cornell) for CT scan and grants that funded the CT (NIH S10OD012287 for the ZEISS/Xradia Versa 520 X-ray Microscope, and NIH S10OD025049 for the SkyScan 1276); Kemper Lewis and Department of Mechanical and Aerospace Engineering (University at Buffalo (UB)) for access to ANSYS; Noreen von Cramon-Taubadel and Evan Simons (UB) for helpful comments on the morphometric analysis; and Delfine Cheng (Victor Chang Cardiac Research Institute) for inviting us to submit this manuscript. JL acknowledges Open Grant from State Key Laboratory of Palaeobiology and Stratigraphy (Nanjing Institute of Geology and Palaeontology, Chinese Academy of Sciences) (173116); JMN acknowledges the CERCA programme of the Generalitat de Catalunya.

References

Adams, D.C., Otárola-Castillo, E., 2013. geomorph: an < scp > r < /scp > package for the collection and analysis of geometric morphometric shape data. Methods Ecol. Evol. 4, 393–399. https://doi.org/10.1111/2041-210X.12035.

Alexander, R.M., 1962. The structure of the Weberian apparatus in the Cyprini. Proc. Zool. Soc. London 139, 451–473. https://doi.org/10.1111/j.1469-7998.1962.tb01839.x.

Alexander, R.M., 1959. The densities of Cyprinidae. J Exp Biol 36, 333–340.

Areias, B., Santos, C., Natal Jorge, R.M., Gentil, F., Parente, M.P.L., 2016. Finite element modelling of sound transmission from outer to inner ear. Proc. Inst. Mech. Eng. Part H J. Eng. Med 230, 999–1007. https://doi.org/10.1177/0954411916666109.

Babaei, F., Hong, T.L.C., Yeung, K., Cheng, S.H., Lam, Y.W., 2016. Contrast-Enhanced X-Ray Micro-Computed Tomography as a Versatile Method for Anatomical Studies of Adult Zebrafish. Zebrafish 13, 310–316. https://doi.org/10.1089/zeb.2016.1245.

Baker, T.R., Peterson, R.E., Heideman, W., 2013. Early Dioxin Exposure Causes Toxic Effects in Adult Zebrafish. Toxicol. Sci. 135, 241–250. https://doi.org/10.1093/toxsci/kft144.

Barbero, B.R., Ureta, E.S., 2011. Comparative study of different digitization techniques and their accuracy. CAD Comput. Aided Des. 43, 188–206. https://doi.org/10.1016/j.cad.2010.11.005.

Bird, N.C., Hernandez, L.P., 2009. Building an evolutionary innovation: Differential growth in the modified vertebral elements of the zebrafish Weberian apparatus. Zoology 112, 97–112. https://doi.org/10.1016/j.zool.2008.05.003.

Bird, N.C., Mabee, P.M., 2003. Developmental Morphology of the Axial Skeleton of the Zebrafish, Danio rerio (Ostariophysi: Cyprinidae). Dev. Dyn. 228, 337–357. https://doi.org/10.1002/dvdy.10387.

Blanco-Sánchez, B., Clément, A., Phillips, J.B., Westerfield, M., 2017. Zebrafish models of human eye and inner ear diseases. 415–467. https://doi.org/10.1016/bs.mcb.2016.10.006.

Brown, D.D., 1997. The role of thyroid hormone in zebrafish and axolotl development. Proc. Natl. Acad. Sci. 94, 13011–13016. https://doi.org/10.1073/pnas.94.24.13011.

Caminos, L., Garcia-Manrique, J., Lima-Rodriguez, A., Gonzalez-Herrera, A., 2018. Analysis of the Mechanical Properties of the Human Tympanic Membrane and Its Influence on the Dynamic Behaviour of the Human Hearing System. Appl. Bionics Biomech. 2018, 1–12. https://doi.org/10.1155/2018/1736957.

Cheng, K.C., Xin, X., Clark, D.P., La Riviere, P., 2011. Whole-animal imaging, gene function, and the Zebrafish Phenome Project. Curr. Opin. Genet. Dev. 21, 620–629. https://doi.org/10.1016/j.gde.2011.08.006.

Cubbage, C.C., Mabee, P.M., 1996. Development of the cranium and paired fins in the zebrafishDanio rerio (Ostariophysi, Cyprinidae). J. Morphol. 229, 121–160. https://doi.org/10.1002/(SICI)1097-4687(199608)229:2<121::AID-JMOR1>3.0.CO;2-4.

Curtis, N., 2011. Craniofacial biomechanics: An overview of recent multibody modelling studies. J. Anat. 218, 16–25. https://doi.org/10.1111/j.1469-7580.2010.01317.x.

Davies, T.G., Rahman, I.A., Lautenschlager, S., Cunningham, J.A., Asher, R.J., Barrett, P.M., Bates, K.T., Bengtson, S., Benson, R.B.J., Boyer, D.M., Braga, J., Bright, J.A., Claessens, L.P.A.M., Cox, P.G., Dong, X.-P., Evans, A.R., Falkingham, P.L., Friedman, M., Garwood, R.J., Goswami, A., Hutchinson, J.R., Jeffery, N.S., Johanson, Z., Lebrun, R., Martínez-Pérez, C., Marugán-Lobón, J., O'Higgins, P.M., Metscher, B., Orliac, M., Rowe, T.B., Rücklin, M., Sánchez-Villagra, M.R., Shubin, N.H., Smith, S.Y., Starck, J.M., Stringer, C., Summers, A.P., Sutton, M.D., Walsh, S.A., Weisbecker, V., Witmer, L.M., Wroe, S., Yin, Z., Rayfield, E.J., Donoghue, P.C.J., 2017. Open data and digital morphology. Proc. R. Soc. B Biol. Sci. 284, 20170194. https://doi.org/10.1098/rspb.2017.0194.

De Greef, D., Aernouts, J., Aerts, J., Cheng, J.T., Horwitz, R., Rosowski, J.J., Dirckx, J.J.J., 2014. Viscoelastic properties of the human tympanic membrane studied with stroboscopic holography and finite element modeling. Hear. Res. 312, 69–80. https://doi.org/10.1016/j.heares.2014.03.002.

De Greef, D., Pires, F., Dirckx, J.J.J., 2017. Effects of model definitions and parameter values in finite element modeling of human middle ear mechanics. Hear. Res. 344, 195–206. https://doi.org/10.1016/j.heares.2016.11.011.

Ding, Y., Vanselow, D.J., Yakovlev, M.A., Katz, S.R., Lin, A.Y., Clark, D.P., Vargas, P., Xin, X., Copper, J.E., Canfield, V.A., Ang, K.C., Wang, Y., Xiao, X., De Carlo, F., van Rossum, D.B., La Riviere, P., Cheng, K.C., 2019. Computational 3D histological phenotyping of whole zebrafish by X-ray histotomography. Elife 8, 1–28. https://doi.org/10.7554/eLife.44898.

Engelkes, K., Helfsgott, J., Hammel, J.U., Büsse, S., Kleinteich, T., Beerlink, A., Gorb, S.N., Haas, A., 2019. Measurement error in μCT-based three-dimensional geometric morphometrics introduced by surface generation and landmark data acquisition. J. Anat. https://doi.org/10.1111/joa.12999.

Evans, H.M., 1925. A Contribution to the Anatomy and Physiology of the Air-Bladder and Weberian Ossicles in Cyprinidae. Proc. R. Soc. B Biol. Sci. 97, 545–576. https://doi.org/10.1098/rspb.1925.0018.

Finneran, J.J., Hastings, M.C., 2000. A mathematical analysis of the peripheral auditory system mechanics in the goldfish (Carassius auratus). J. Acoust. Soc. Am. 108, 1308. https://doi.org/10.1121/1.1286099.

Fisher, S., Mabee, P.M., 2004. Skeletogenesis in Zebrafish Danio rerio. Evolutionary and Developmental Aspects. pp 392–423. https://doi.org/10.1142/9789812565761_0011.

Fleming, A., Sato, M., Goldsmith, P., 2005. High-Throughput In Vivo Screening for Bone Anabolic Compounds with Zebrafish. J. Biomol. Screen. 10, 823–831. https://doi.org/10.1177/1087057105279952.

Funnell, W.R.J., Khanna, S.M., Decraemer, W.F., 1992. On the degree of rigidity of the manubrium in a finite-element model of the cat eardrum. J. Acoust. Soc. Am. 91, 2082–2090. https://doi.org/10.1121/1.403694.

Grande, T., Young, B., 2004. The ontogeny and homology of the Weberian apparatus in the zebrafish Danio rerio (Ostariophysi: Cypriniformes). Zool. J. Linn. Soc. 140, 241–254. https://doi.org/10.1111/j.1096-3642.2003.00097.x.

Harris, M.P., Henke, K., Hawkins, M.B., Witten, P.E., 2014. Fish is Fish: The use of experimental model species to reveal causes of skeletal diversity in evolution and disease. J. Appl. Ichthyol. 30, 616–629. https://doi.org/10.1111/jai.12533.

Hernandez, L.P., Bird, N.C., Staab, K.L., 2007. Using zebrafish to investigate cypriniform evolutionary novelties: functional development and evolutionary diversification of the kinethmoid. J. Exp. Zool. Part B Mol. Dev. Evol. 308B, 625–641. https://doi.org/10.1002/jez.b.21166.

Higgs, D.M., Rollo, A.K., Souza, M.J., Popper, A.N., 2003. Development of form and function in peripheral auditory structures of the zebrafish (Danio rerio). J. Acoust. Soc. Am. 113, 1145–1154. https://doi.org/10.1121/1.1536185.

Hur, M., Gistelinck, C.A., Huber, P., Lee, J., Thompson, M.H., Monstad-Rios, A.T., Watson, C.J., McMenamin, S.K., Willaert, A., Parichy, D.M., Coucke, P., Kwon, R.Y., 2017. MicroCT-based phenomics in the zebrafish skeleton reveals virtues of deep phenotyping in a distributed organ system. Elife 6, 1–23. https://doi.org/10.7554/eLife.26014.

Keer, S., Cohen, K., May, C., Hu, Y., McMenamin, S., Hernandez, L.P., 2019. Anatomical Assessment of the Adult Skeleton of Zebrafish Reared Under Different Thyroid Hormone Profiles. Anat. Rec. 302, 1754–1769. https://doi.org/10.1002/ar.24139.

Ladich, F., Fay, R.R., 2013. Auditory evoked potential audiometry in fish. Reviews in Fish Biology and Fisheries. https://doi.org/10.1007/s11160-012-9297-z.

Ladich, F., Wysocki, L.E., 2003. How does tripus extirpation affect auditory sensitivity in goldfish? Hear. Res. 182, 119–129. https://doi.org/10.1016/S0378-5955(03)00188-6.

Lechner, W., Ladich, F., 2008. Size matters: diversity in swimbladders and Weberian ossicles affects hearing in catfishes. J. Exp. Biol. 211, 1681–1689. https://doi.org/10.1242/jeb.016436.

Marcé-Nogué, J., Fortuny, J., Gil, L., Galobart, A., 2011. Using reverse engineering to reconstruct tetrapod skulls and analyse its feeding behaviour. Proc. 13th Int. Conf. Civil, Struct. Environ. Eng. Comput 1–12. https://doi.org/10.4203/ccp.96.237.

Marcé-Nogué, J., Fortuny, J., Gil, L., Sánchez, M., 2015. Improving mesh generation in Finite Element Analysis for functional morphology approaches. Spanish J. Palaeontol. 31, 117–132.

Marcy, A.E., Fruciano, C., Phillips, M.J., Mardon, K., Weisbecker, V., 2018. Low resolution scans can provide a sufficiently accurate, cost- and time-effective alternative to high resolution scans for 3D shape analyses. PeerJ 6, e5032. https://doi.org/10.7717/peerj.5032.

McCurry, M.R., Evans, A.R., McHenry, C.R., 2015. The sensitivity of biological finite element models to the resolution of surface geometry: a case study of crocodilian crania. PeerJ 3, e988. https://doi.org/10.7717/peerj.988.

Metscher, B.D., 2009. Micro CT for comparative morphology: Simple staining methods allow high-contrast 3D imaging of diverse non-mineralized animal tissues. BMC Physiol 9. https://doi.org/10.1186/1472-6793-9-11.

Neues, F., Arnold, W.H., Fischer, J., Beckmann, F., Gaengler, P., Epple, M., 2006. The skeleton and pharyngeal teeth of zebrafish (Danio rerio) as a model of biomineralization in vertebrates. Materwiss. Werksttech. 37, 426–431. https://doi.org/10.1002/mawe.200600009.

Nicolson, T., 2017. The genetics of hair-cell function in zebrafish. J. Neurogenet. 31, 102–112. https://doi.org/10.1080/01677063.2017.1342246.

Piegl, L., Tiller, W., 1997. The NURBS book, 2nd edition. Springer-Verlag.

Polly, P.D., Stayton, C.T., Dumont, E.R., Pierce, S.E., Rayfield, E.J., Angielczyk, K.D., 2016. Combining geometric morphometrics and finite element analysis with evolutionary modeling: towards a synthesis. J. Vertebr. Paleontol. 36. https://doi.org/10.1080/02724634.2016.1111225.

Popper, A.N., 1972. Pure-Tone Auditory Thresholds for the Carp, Cyprinis carpio. J. Acoust. Soc. Am. 52, 1714–1717. https://doi.org/10.1121/1.1913305.

Popper, A.N., Fay, R.R., 2011. Rethinking sound detection by fishes. Hear. Res. 273, 25–36. https://doi.org/10.1016/j.heares.2009.12.023.

Rahman, I.A., 2017. Computational fluid dynamics as a tool for testing functional and ecological hypotheses in fossil taxa. Palaeontology 60, 451–459. https://doi.org/10.1111/pala.12295.

Rayfield, E.J., 2007. Finite Element Analysis and Understanding the Biomechanics and Evolution of Living and Fossil Organisms. Annu. Rev. Earth Planet. Sci. 35, 541–576. https://doi.org/10.1146/annurev.earth.35.031306.140104.

Retzius, G., 1881. Das Gehörorgan der Wirbelthiere: morphologisch-histologische Studien. Samson Wallin, Stockholm.

Siomava, N., Shkil, F., Voronezhskaya, E., Diogo, R., 2018. Development of zebrafish paired and median fin musculature: basis for comparative, developmental, and macroevolutionary studies. Sci. Rep. 8, 1–16. https://doi.org/10.1038/s41598-018-32567-z.

Soons, J.A.M., Aernouts, J., Dirckx, J.J.J., 2010. Elasticity modulus of rabbit middle ear ossicles determined by a novel micro-indentation technique. Hear. Res. 263, 33–37. https://doi.org/10.1016/j.heares.2009.10.001.

Sutton, M., Rahman, I.A., Garwood, R., 2016. Virtual Paleontology—an Overview. Paleontol. Soc. Pap. 22, 1–20. https://doi.org/10.1017/scs.2017.5.

Volandri, G., Di Puccio, F., Forte, P., Carmignani, C., 2011. Biomechanics of the tympanic membrane. J. Biomech. 44, 1219–1236. https://doi.org/10.1016/j.jbiomech.2010.12.023.

Walter, T., Shattuck, D.W., Baldock, R., Bastin, M.E., Carpenter, A.E., Duce, S., Ellenberg, J., Fraser, A., Hamilton, N., Pieper, S., Ragan, M.A., Schneider, J.E., Tomancak, P., Hériché, J.K., 2010. Visualization of image data from cells to organisms. Nat. Methods 7, S26–S41. https://doi.org/10.1038/nmeth.1431.

Weatherill, N., Soni, B., Thompson, J., 1998. Handbook of Grid Generation, Handbook of Grid Generation. CRC Press. https://doi.org/10.1201/9781420050349.

Weber, E.H., 1820. De Aure et Auditu Hominis et Animalium: Pars 1 De aure Animalium Aquatilium. Leipzig.

Weigele, J., Franz-Odendaal, T.A., 2016. Functional bone histology of zebrafish reveals two types of endochondral ossification, different types of osteoblast clusters and a new bone type. J. Anat. 229, 92–103. https://doi.org/10.1111/joa.12480.

Whitfield, T.T., 2002. Zebrafish as a model for hearing and deafness. J. Neurobiol. 53, 157–171. https://doi.org/10.1002/neu.10123.